Synthesis of Silver Octahedra with Controlled Sizes and Optical Properties *via* Seed-Mediated Growth

Yi Wang,[†,‡] Dehui Wan,[†] Shuifen Xie,[†] Xiaohu Xia,[†] Cheng Zhi Huang,[‡] and Younan Xia[†,§,*]

[†]The Wallace H. Coulter Department of Biomedical Engineering, Georgia Institute of Technology and Emory University, Atlanta, Georgia 30332, United States, [‡]Education Ministry Key Laboratory on Luminescence and Real-Time Analysis, College of Chemistry and Chemical Engineering, Southwest University, Chongqing 400715, P. R. China, and [§]School of Chemistry and Biochemistry, School of Chemical and Biomolecular Engineering, Georgia Institute of Technology, Atlanta, Georgia 30332, United States

ABSTRACT Silver octahedra with edge lengths controlled in the range of 20–72 nm were synthesized *via* seed-mediated growth. The key to the success of this synthesis is the use of single-crystal Ag seeds with uniform and precisely controlled sizes to direct the growth and the use of citrate as a selective capping agent for the {111} facets. Our mechanistic studies demonstrated that Ag seeds with both cubic and quasi-spherical shapes could evolve into octahedra. For the first time, we were able to precisely control the edge lengths of Ag octahedra below 100 nm, and the lower limit of size could even be pushed down to 20 nm. Using the as-obtained Ag octahedra as sacrificial templates, Au nanocages with an octahedral shape and precisely tunable optical properties were synthesized through a galvanic replacement reaction. Such hollow nanostructures are promising candidates for a broad range of applications related to optics, catalysis, and biomedicine.

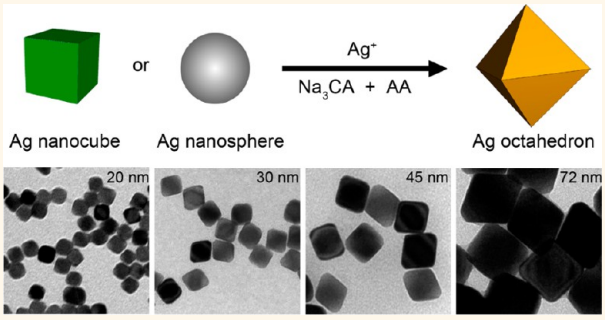

KEYWORDS: silver nanocrystal · octahedron · seed · size control · nanocage

Silver has been widely used as a selective catalyst (*e.g.*, for ethylene epoxidation) in industry and an effective antibacterial agent in biomedicine.[1−5] It is also of great interest as optical components or probes for potential applications related to surface-enhanced Raman scattering and localized surface plasmon resonance (LSPR).[6−11] Therefore, controlling both the size and shape of Ag nanocrystals has received extensive attention in recent years since these two parameters allow researchers to tailor the intrinsic properties, thus, enhancing their performance in a broad range of applications. To date, there have been many successful demonstrations in the synthesis of Ag nanocrystals with a wide variety of shapes, including sphere, cube, bar, octahedron, bipyramid, decahedron, rod/wire with a pentagonal cross section, and concave structures enclosed by high-index facets.[10−13] Most of these shape-controlled nanocrystals are still troubled by issues such as low yield/purity, unsatisfactory uniformity, poor reproducibility, and lack of effective means to precisely control the size while keeping the shape for a specific application. Exceptions are Ag nanocubes and nanowires because both of them can now be produced using the polyol method in high yield/purity, large quantity, as well as good uniformity and precisely controlled sizes.[14−19] In addition, Mirkin and co-workers have also successfully synthesized Ag nanoprisms (or nanoplates) with controlled sizes and Ag nanorods with controlled aspect ratios through a photochemical method.[20−22]

Different from Ag nanocubes enclosed by {100} facets, Ag octahedra are completely covered by {111} facets and have much lower surface free energy and thus exhibit quite different properties. For example, Christopher and Linic reported that the {100} and {111} facets of Ag had distinct catalytic selectivity for the ethylene epoxidation owing to the difference in activation barrier for the formation of ethylene oxide and acetaldehyde on the two different facets.[1,2] Yang and co-workers reported that Ag polyhedrons enclosed by different ratios

* Address correspondence to younan.xia@bme.gatech.edu.

Received for review March 18, 2013 and accepted April 25, 2013.

Published online April 25, 2013
10.1021/nn401363e

of {100}/{111} facets showed distinct LSPR scattering signatures.[23] To achieve a systematic comparison with Ag nanocubes 18−200 nm in size,[14−16] synthesis of Ag octahedra with precisely controlled sizes in the same range is also of great significance for various applications. So far, there have been only a few reports on the syntheses of Ag octahedra with uniform sizes. To this end, Yang and co-workers have prepared Ag octahedra in 1,5-pentanediol, where Ag precursor and stabilizer were injected periodically into a solution containing presynthesized Ag nanocubes.[23−26] Tsuji and co-workers synthesized Ag octahedra in *N*,*N*-dimethylformamide, but the octahedra in their final products seemed to be pretty low in yield.[27] It should be pointed out that the sizes of the Ag octahedra reported in all of these studies were larger than 150 nm. Smaller Ag octahedra with well-controlled sizes (especially for the sizes below 100 nm) and in high purity seem to be very hard to prepare, which can be attributed to the following two possible reasons: (i) the lack of a reliable method to synthesize small, high-purity, and uniform single-crystal Ag seeds for further growth into Ag octahedra with relatively small sizes. In general, once the formation of Ag seeds is initiated, it is hard to terminate until the precursor has been consumed due to the fact that the growth of Ag is autocatalytic.[14,28,29] (ii) The lack of effective capping agent to confine the Ag nanocystals in small sizes and with a specific facet. The interaction between a capping agent and metal surfaces can change the order of surface free energies for different crystallographic planes of a crystal, and thus allow the growth deviated from a thermodynamically controlled pathway.[12,30−32]

We recently demonstrated that these two issues could be addressed by using seed-mediated growth in the presence of a selective capping agent for the {111} facets.[33] Both theoretical and experimental studies have demonstrated that citrate has a stronger binding to the {111} facets of Ag relative to other types of facets,[33,34] which could be employed to confine the growth of Ag octahedra. Here, we further extend the capability of this new approach by combining it with recent advancement in seed synthesis. More specifically, we have developed a facile and robust method for generating single-crystal Ag seeds with tightly controlled sizes less than 30 nm by manipulating the reduction kinetics in a polyol synthesis.[14] The advantages of the newly prepared Ag seeds, including small and precisely controlled sizes, high purity and uniformity, as well as large quantity per batch, make them excellent seeds for further growth into Ag octahedra with relatively small sizes and in high purity. Because of the excellent seeds and effective capping agent, we obtained Ag octahedra with controlled sizes below 100 nm, together with a narrow size distribution and high purity in shape. Our studies also demonstrated that both cubic and quasi-spherical single-crystal Ag seeds could evolve into octahedra whose sizes were largely determined by the sizes of the seeds we used. In principle, Ag octahedra with sizes ranging from tens of nanometers to a few hundred nanometers can be easily synthesized using the present protocol. In this work, we only focus on the size control of Ag octahedra less than 100 nm because larger ones could be easily prepared. It should be pointed out that this work represents the first demonstration to precisely control the sizes of Ag octahedra below 100 nm, and the lower limit could even be pushed down to 20 nm. The "size" in this article refers to the diameter of a quasi-sphere, the edge length of a cube, or the edge length of an octahedron. Using the as-obtained Ag octahedra as sacrificial templates, Au nanocages with an octahedral shape and tunable optical properties from the visible to the near-infrared region were also synthesized using a galvanic replacement reaction.

RESULTS AND DISCUSSION

Comparison of Different Seeds for the Synthesis of Ag Octahedra. The synthesis of Ag octahedra was conducted in an aqueous solution *via* seed-mediated growth, with single-crystal Ag nanocubes and quasi-spheres relatively small in size as the seeds, respectively. During the growth of Ag octahedra, specific amounts of silver trifluoroacetate (CF_3COOAg), L-ascorbic acid (AA), and sodium citrate (Na_3CA) were introduced into the presynthesized Ag seeds. These chemicals served as the precursor, reductant, and capping agent, respectively. The transmission electron microscopy (TEM) images in Figure 1 shows the evolution from cubic Ag seeds into octahedra. The cubic seeds with a uniform size (45 ± 3.5 nm in edge length) were obtained *via* an ethylene glycol (EG)-based polyol synthesis. After adding 0.8 mL of Ag precursor through a syringe pump, Ag nanocubes with truncation at corners were obtained, suggesting that the growth was mainly along the ⟨100⟩ direction of the cubic seeds. Further growth of these truncated nanocubes led to the formation of cuboctahedrons, truncated octahedra, and octahedra after 1.1, 1.4, and 1.7 mL of the CF_3COOAg solution had been introduced, respectively. This result suggests that the newly formed Ag atoms were mainly deposited on the {100} facets, making the proportion of {111} facets constantly enlarged at the expense of {100} facets, which eventually disappeared. It should be pointed out that Ag nanocrystals tend to lose their sharp corners/edges due to the sensitivity of Ag toward oxidative etching caused by the oxygen from air, especially when they are relatively small in size.[14] As a result, the final Ag octahedra of this work showed slight truncation at the corners. We also recorded TEM images from these Ag polyhedrons at different tilting angles (from −30° to 30°) relative to the electron beam to confirm their structures (Supporting Information, Figure S1). Further

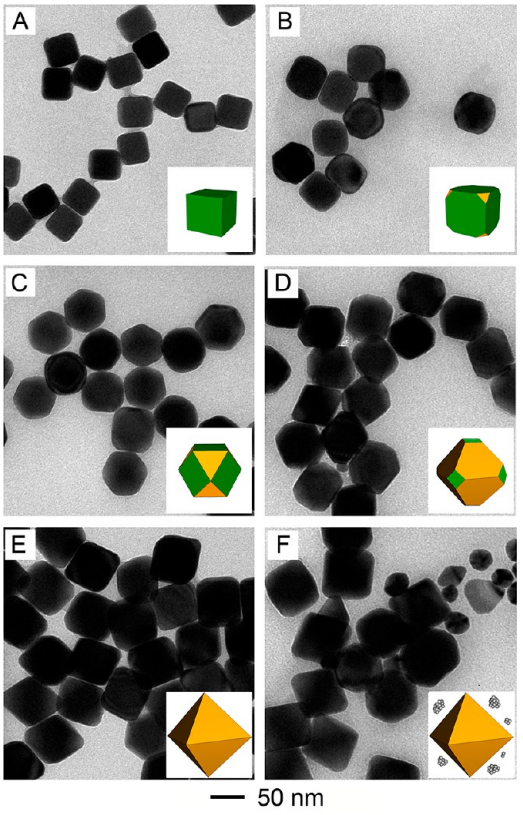

Figure 1. TEM images showing the shape-evolution of single-crystal, cubic Ag seeds into octahedra under the standard condition. The volume of CF_3COOAg (0.3 mM) added into the growth solution was (A) 0, (B) 0.8, (C) 1.1, (D) 1.4, (E) 1.7, and (F) 2.0 mL, respectively. The insets show the corresponding 3D models for the polyhedrons.

growth on the resultant Ag octahedra was not observed when 2.0 mL of the CF_3COOAg solution was added into the system. Instead, irregular Ag nanoparticles started to appear in the product due to the homogeneous nucleation and growth. More and larger irregular Ag particles were obtained in the product with the addition of more (2.4 mL) precursors (Figure S2). This result suggests that homogeneous nucleation was more favorable than heterogeneous nucleation once the octahedra had been formed in the reaction solution. Generally, the energy barrier for heterogeneous nucleation would be lower than that for homogeneous nucleation.[35] In the present system, however, the energy barrier for further deposition of Ag atoms onto the {111} facets of an octahedron was higher than that for self-nucleation. This difference can be attributed to the capping effect of citrate on the {111} facets of Ag nanocrystals, which can greatly increase the energy barrier for nucleation on these facets. We also observed a similar phenomenon of self-termination for Pd octahedra.[36]

When Ag quasi-spheres of 35 ± 3.2 nm in size were used as the seeds, the shape-evolution during their growth was slightly different from the cubic seeds (Figure 2). Unlike the cubic Ag seeds fully enclosed

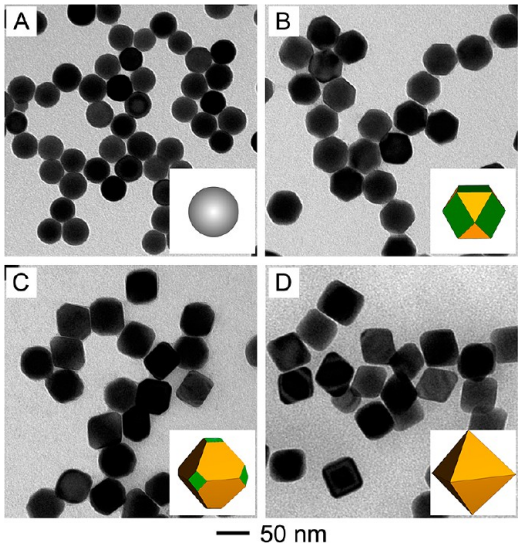

Figure 2. TEM images showing the shape-evolution of single-crystal, quasi-spherical Ag seeds into octahedra with the standard procedure. The volume of CF_3COOAg (0.3 mM) added into the growth solution was (A) 0, (B) 0.5, (C) 0.8, and (D) 1.0 mL, respectively. The insets illustrate the corresponding 3D models for the polyhedrons.

by {100} facets, the quasi-spherical Ag nanocrystals were covered by a mix of {100} and {111} facets. Compared with the seeds, Ag cuboctahedrons with better resolved boundaries between the {100} and {111} facets were first obtained when 0.5 mL of the CF_3COOAg solution was added. Further growth of the cuboctahedrons was similar to the case of cubic seeds, leading to the formation of truncated octahedra and octahedra after 0.8 and 1.0 mL of the CF_3COOAg solution had been added, respectively. Similarly, irregular Ag particles were also obtained together with the Ag octahedra due to the homogeneous nucleation and growth when too much CF_3COOAg solution was added (Figure S3). These results indicate that Ag octahedra fully enclosed by {111} facets can be easily obtained using the present protocol, regardless of the shape for the single-crystal Ag seeds. Figure S4 shows high-resolution TEM (HRTEM) images of the typical Ag seeds and one of the as-obtained Ag octahedra. The fringe spacing of 1.4, 2.0, and 2.36 Å on the surfaces of the nanocrystals can be indexed to the {220}, {200}, and {111} reflections of face-centered cubic (*fcc*) Ag, respectively. The Fourier transform (FT) patterns obtained from the corresponding nanocrystals further confirmed that the seeds and the products were all single crystals in structure. To better understand the correlation between the crystallinity of seeds and the products, we also conducted a set of syntheses involving multiply twinned Ag seeds for comparison. The result shows that multiply twinned Ag particles were obtained when twinned Ag seeds were employed for the seed-mediated growth (Figure S5). Combined together, we can conclude that the use of

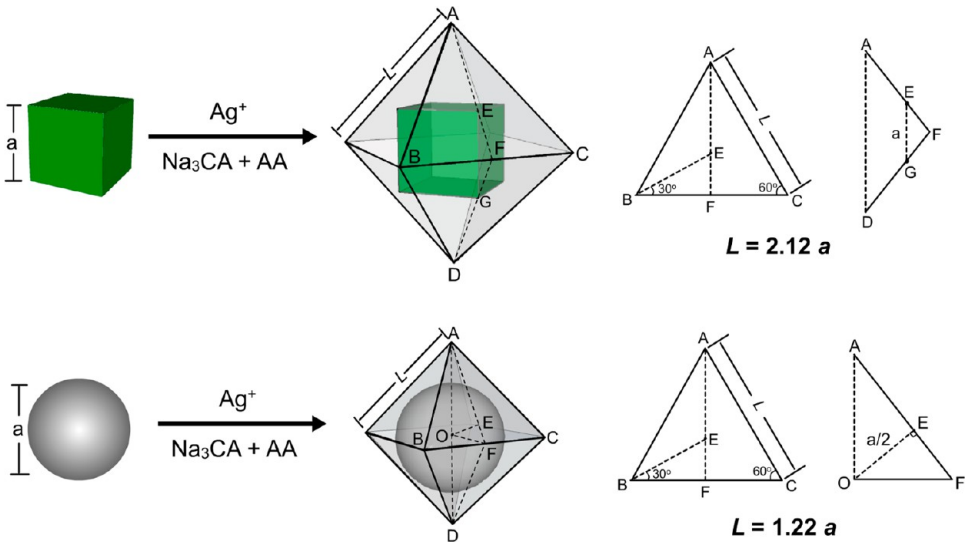

Figure 3. Seed-mediated growth of Ag octahedra from single-crystal cubic and quasi-spherical seeds of Ag, respectively. The size (*L*) of the resultant Ag octahedra is determined by the size (*a*) of the cubic or quasi-spherical seed. The "size" refers to the diameter of a quasi-spherical seed and the edge length of a cubic seed.

high-purity single-crystal Ag seeds for the growth is a crucial parameter in the formation of Ag octahedra with good quality and purity in the present work.

Regardless of the shape of the single-crystal Ag seeds used for the synthesis of Ag octahedra, the size of the resultant octahedra is largely determined by the size of the seeds. In an ideal situation where growth is limited to the ⟨100⟩ direction only, the sizes of the octahedra and the cubic seeds should be related by a factor of 2.12 (Figure 3, top trace). If quasi-spherical Ag seeds are used for growth in the same way, the smallest size of the resultant octahedra should be 1.22 times of the size of the seeds (Figure 3, bottom trace). The details of size calculation for octahedra grown from cubic and quasi-spherical seeds, respectively, are shown in Figure S6 of the Supporting Information. However, from the TEM images shown in Figure 1, we found that the average size (72 ± 5.0 nm) of the resultant Ag octahedra was smaller than the size (95 nm) calculated for the octahedra grown from cubic seeds of 45 nm in edge length under an ideal situation. This discrepancy in size is similar to our previous observations and the results from other groups,[27,37] which could be attributed to the slight truncation at the corners of the cubic seeds. For the octahedra grown from Ag quasi-spherical seeds (35 ± 3.2 nm in diameter), the size of 43 ± 3.8 nm was close to what we calculated for the ideal situation (Figure 2).

We also recorded UV−vis spectra of the Ag polyhedrons shown in Figures 1 and 2, which allowed us to systematically study the effects of the size and shape of Ag nanocrystals on LSPR properties. As shown in Figure 4A, the 45-nm cubic Ag seeds had three LSPR peaks located at 350, 380, and 440 nm, which are identical with our previous studies.[15,16] In comparison with the cubic seeds, the peak at 380 nm disappeared and only

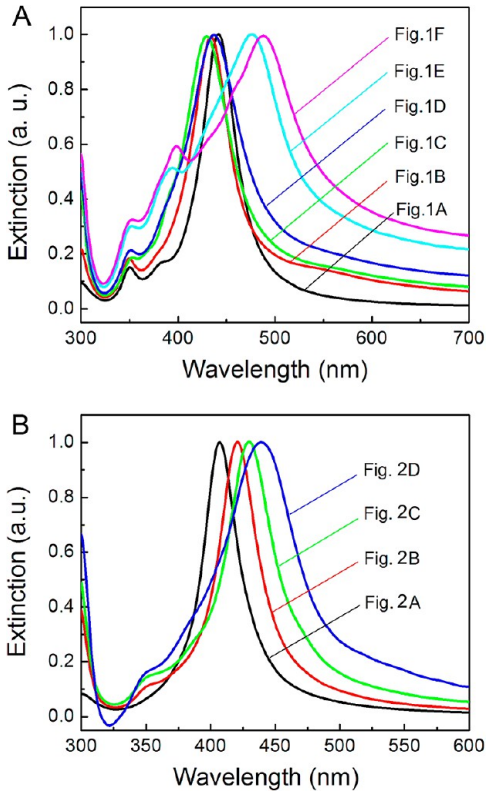

Figure 4. Normalized extinction spectra of the Ag polyhedrons shown in Figures 1 and 2.

two peaks could be observed for the truncated cubes and cuboctahedrons, which might be due to their higher symmetry than the cubes. Thereafter, the peak at ~380 nm appeared again when the truncated octahedra and octahedra formed, indicating that this peak was associated with the dipole resonance of the sharp corners/edges. For the 35-nm spherical Ag seeds, only one LSPR peak located at 407 nm was observed

due to the high isotropy (Figure 4B). When cuboctahedrons were formed, another peak at 350 nm started to appear. Then, three peaks were observed as the truncated octahedra and octahedra were formed, which was similar to the case of cubic seeds. These observations agree well with the results obtained from the discrete dipole approximation (DDA) calculations, where the number of resonance peaks exhibited by a metal polyhedron increases with the number of ways in which it can be polarized (*i.e.*, when the polyhedron has a lower symmetry).[38,39]

Size Control for the Ag Octahedra. Upon the basis of the understanding of the relationship between the size of Ag seeds and the resultant Ag octahedra, we further achieved the syntheses of Ag octahedra with a range of controlled sizes under 100 nm. First, single-crystal cubic or quasi-spherical Ag seeds with uniform sizes and in high purity were prepared using the polyol-based methods.[14,15] Specifically, the seeds of 16 ± 1.5, 21 ± 2.0, and 28 ± 2.0 nm in size were prepared in diethylene glycol (DEG), while the seeds larger than 30 nm in size were obtained in EG. As shown by TEM images in Figure 5, insets of panels A–D, single-crystal Ag seeds with excellent uniformity and purity in both size and shape were obtained. Using seed-mediated growth as a powerful approach, these seeds with different sizes could be grown into Ag octahedra of 20 ± 2.2, 30 ± 2.8, 45 ± 3.5, and 72 ± 5.0 nm in size, respectively (Figure 5A–D). Since we have successfully achieved the synthesis of single-crystal Ag seeds with controlled sizes in the range of 15–200 nm using the polyol method,[14–16] in principle, we could obtain Ag octahedra with sizes in the range of 20–400 nm using the present protocol.

Figure 5E shows UV–vis spectra of the resultant Ag octahedra with different sizes. The major LSPR peaks continuously red-shifted with the increase of particle size. Two peaks located at 350 nm and beyond 400 nm were observed for the 20- or 30-nm Ag octahedra, while another peak located at ~385 nm appeared when the size of the Ag octahedra increased to 45 and 72 nm. The difference in LSPR properties of the octahedra with different sizes are similar to that of Ag nanocubes.[14–16] The major LSPR peaks of the Ag seeds also exhibited a continuous red-shift from 398 to 405, 416, and 440 nm as the size increased (Figure S7).

To obtain Ag octahedra with controlled sizes below 100 nm as well as in high purity and uniformity, one has to fulfill the following two requirements: (i) a tight control of the size of Ag seeds below 50 nm, together with high purity, single-crystallinity, and good uniformity; and (ii) effective capping of the Ag{111} facets to confine the octahedra to small sizes, together with relatively sharp corners/edges and smooth surfaces. Both of the theoretical and experimental studies have shown that citrate can bind more strongly to {111} facets than {100} facets of Ag.[33,34,40] The capping can

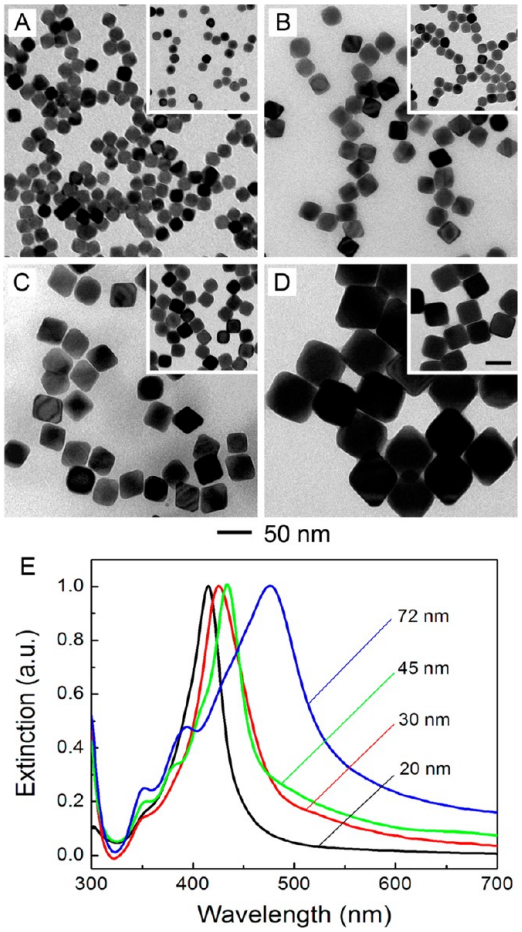

Figure 5. Size control for the Ag octahedra: (A–D) TEM images of Ag octahedra with different edge lengths of (A) 20, (B) 30, (C) 45, and (D) 72 nm; (E) normalized extinction spectra of the Ag octahedra as shown in panels A–D. The insets of panels A–D show the corresponding Ag quasi-spherical seeds of 16 nm and cubic seeds of 21, 28, and 45 nm in size, respectively. The scale bar in the inset of panel D is 50 nm and applies to all other insets.

facilitate the growth of Ag along ⟨100⟩ direction and meanwhile exposes {111} facets. As a result, the {100} facets gradually disappeared while the {111} facets became more dominant and eventually formed the Ag octahedra. Moreover, our results also show that only Ag octahedra with rounded corners/edges could be obtained when the amount of citrate was reduced to $^1/_{10}$ of the standard synthesis (Figure S8A), demonstrating the important role of citrate for effective capping of the Ag{111} facets. When Ag octahedra were employed as seeds for further growth in the presence of citrate at a number of concentrations, the final products were mixtures of the original seeds and irregular nanoparticles formed through self-nucleation (Figure S8B). Combined together, the key to the successful synthesis of Ag octahedra with controlled sizes and in high purity is the use of Ag seeds with precisely controlled sizes and high quality as well as the use of an effective capping agent, citrate, for the {111} facets of Ag.

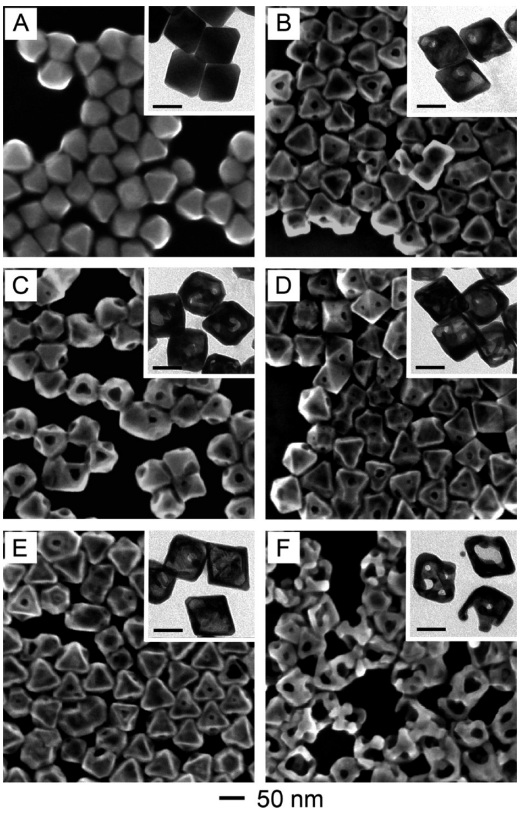

Figure 6. SEM images showing the galvanic replacement reaction between Ag octahedra and 0.1 mM $HAuCl_4$ after different volumes of this solution had been added: (A) 0, (B) 1.0, (C) 2.0, (D) 3.0, (E) 5.0, and (F) 7.0 mL. Insets show the corresponding TEM images and the scale bars are 50 nm.

Synthesis of Au Octahedral Nanocages with Tunable Optical Properties. Hollow metal nanostructures have attracted increasing attention in resent years due to their unique properties and great performances in a variety of applications such as catalysis and biomedicine.[41−44] Galvanic replacement reaction has been demonstrated to be a simple and effective method for preparation of metallic nanostructures with hollow interiors and porous walls. To date, we have successfully achieved the synthesis of Au, Pd, and Pt nanocages/nanoboxes with different features for a variety of applications, using Ag nanocubes enclosed by {100} facets as sacrificial templates.[45−51] Herein, it is interesting to investigate the galvanic replacement reaction on nanocrystals with an octahedral shape and thus fully enclosed by {111} facets. Figure 6 shows SEM and TEM (insets) images of Ag octahedra before and after they had reacted with 0.1 mM $HAuCl_4$ at different volumes at 90 °C. We used Ag octahedra of 72 nm in size as the templates. As shown in Figure 6A, Ag octahedra with smooth surfaces can be clearly observed. After they had reacted with 1.0 mL of $HAuCl_4$, small holes were generated at the side faces of the Ag octahedra (Figure 6B), indicating that the galvanic replacement reaction was initiated on the {111} facets. This observation is consistent with our previous report that the

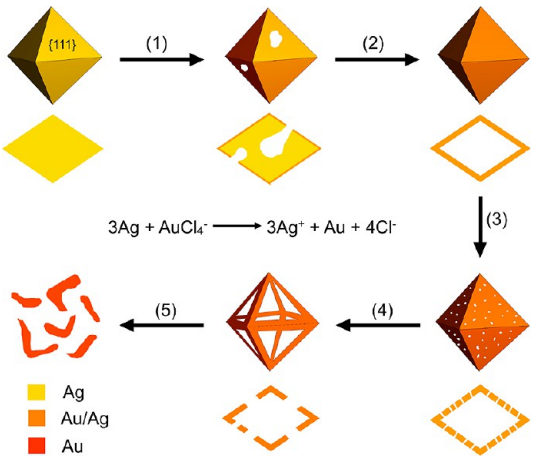

Figure 7. Schematic illustration showing the morphological and structural evolution involved in the galvanic replacement reaction between an Ag octahedron and aqueous $HAuCl_4$ solution.

corner regions of a truncated nanocube terminated in {111} facets served as the primary sites for galvanic replacement reaction.[49] At this stage, Ag atoms could be oxidized by Au^{3+} to form Ag^+ and escaped from the holes. Meanwhile, Au^{3+} was reduced to Au atoms and deposited on the surface of each octahedron as a thin shell. Along with the increase of $HAuCl_4$, larger holes on the surfaces could be generated (Figure 6C). Once the thickness of the Au layer had reached a critical value, these holes would start to shrink (Figure 6D). As a result, all the holes on the surface gradually disappeared to generate nanoboxes with smooth walls and hollow interiors. It should be pointed out that alloying always occurred between the deposited Au layer and the underlying Ag surface due to the high diffusion rates of Au and Ag atoms at such high temperature (90 °C).[52] When the $HAuCl_4$ solution was increased to 5.0 mL, dealloying of the nanoboxes occurred to generate octahedral nanocages (Figure 6E). Nanoframes were finally obtained when 7.0 mL of $HAuCl_4$ solution was added (Figure 6F), and they started to collapse into Au fragments with the further addition of $HAuCl_4$ (Figure S9).

Figure 7 summarizes the major steps of the galvanic replacement reaction between $HAuCl_4$ and Ag octahedra. Once $HAuCl_4$ solution is added to the dispersion of Ag octahedra, the replacement reaction will start from their {111} facets. Ag atoms start to dissolve from the reaction site, and holes will appear on the surfaces of the octahedra (step 1). During this process, Ag atoms are oxidized and release electrons, which can easily migrate to the surfaces of the octahedron and be used to reduce $AuCl_4^-$ into Au atoms. The generated Au atoms tend to be deposited on the surfaces of each template to form a thin layer due to a good matching of the crystal lattices between Au and Ag (4.0786 and 4.0862 Å for Au and Ag, respectively). As the amount of $HAuCl_4$ increases, the surfaces containing holes will act

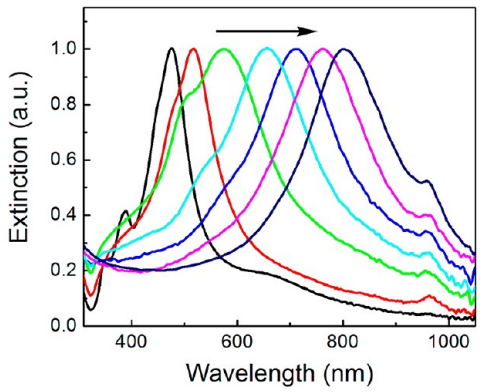

Figure 8. Normalized extinction spectra showing the galvanic replacement reaction between Ag octahedra and 0.1 mM $HAuCl_4$ solution at different volumes (from left to right: 0, 0.5, 1.0, 2.0, 3.0, 4.5, and 6.0 mL). The LSPR peak positions of the Au octahedral nanoboxes/cages could be precisely tuned across from the visible to the near-infrared region by varying the amount of $HAuCl_4$.

as the most active sites for the further replacement reaction. As a result, the holes become larger and hollow interiors of the template can be obtained. However, when the epitaxial deposition of Au reaches a critical value, these holes will start to shrink, and then gradually disappear to generate nanoboxes with smooth and uniform walls (step 2). Because of the high diffusion rates of Au and Ag atoms at such high temperature (90 °C), more stable Au−Ag alloy will be formed instead of either pure Au shell or Ag inner.[53] If more $HAuCl_4$ is added to the reaction system, the Ag atoms in the Au−Ag nanoboxes will be selectively removed by dealloying process (step 3). Further dealloying will release more Ag atoms into the solution, and some holes will appear again on the surfaces of the nanoboxes due to the lattice vacancies. Then, these holes will coalesce to generate the nanoframes as the $HAuCl_4$ increases (step 4). Complete dealloying will make the nanoframes unable to keep their shape and collapse into small fragments finally (step 5).

By adding different amount of $HAuCl_4$, the LSPR peaks of the Au octahedral nanoboxes/cages could also be precisely tuned. As shown in Figure 8, the Ag octahedra of 72 nm in size exhibit a major LSPR peak at 475 nm, together with two weak peaks at 350 and 392 nm. The major peak of Ag octahedra red-shifted to 517 nm when a small volume of $HAuCl_4$ solution (0.5 mL) was added. It continued to red shift to 575, 655, 710, 760, and 800 nm as 1.0, 2.0, 3.0, 4.5, and 6.0 mL of $HAuCl_4$ solution was added to the reaction system, respectively. Due to their controllable sizes and tunable optical properties (from the visible to the near-infrared region), such Au nanoboxes/cages with octahedral shape could be promising candidates for various applications related to optical sensing, photothermally triggered drug release, and photothermal cancer therapy.

CONCLUSION

We have demonstrated a facile approach to the synthesis of Ag octahedra with precisely controlled sizes using the seed-mediated growth, and further fabricated Au octahedral nanocages with tunable optical properties. Because of the availability of Ag seeds with excellent uniformity, high-purity in shape, and precisely controlled sizes, Ag octahedra with desired sizes below 100 nm could be readily obtained. Since the size of the as-prepared octahedra is determined by the size of the seeds, the present protocol could be used to prepare Ag octahedra with edge lengths in the range of tens of nanometers to a few hundred nanometers. For the first time, we were able to precisely control the edge lengths of Ag octahedra below 100 nm, and the lower limit of size could even be pushed down to 20 nm. Significantly, the Ag octahedra could be confined to relatively small sizes and prepared with sharp corners/edges and smooth surfaces due to the effective capping of citrate for the {111} facets of Ag. We have also demonstrated that both cubic and quasi-spherical seeds could evolve into octahedra *via* seed-mediated growth. Once octahedra had been formed, however, self-nucleation tended to occur if more precursor was added into the reaction solution. In addition, using the as-obtained Ag octahedra as sacrificial templates, Au octahedral nanocages were also synthesized using a galvanic replacement reaction. Owing to their precisely tunable optical properties, such hollow nanostructures are promising candidates for various applications related to optics, catalysis, and biomedicine.

EXPERIMENTAL SECTION

Chemicals and Materials. Silver trifluoroacetate (CF_3COOAg, ≥99.99%), sodium hydrosulfide hydrate ($NaHS \cdot xH_2O$), hydrochloric acid (HCl, 37% in water), poly(vinyl pyrrolidone) (PVP, $M_w \approx 55\,000$), L-ascorbic acid (AA, ≥99.0%), sodium citrate (Na_3CA), diethylene glycol (DEG, ≥99.0%, lot no. BCBF4248V), hydrogen tetrachloroaurate(III) hydrate ($HAuCl_4 \cdot 3H_2O$), acetone, and sodium chloride were all obtained from Sigma-Aldrich. Ethylene glycol (EG) was obtained from J.T. Baker (lot no. G32B27). Deionized (DI) water with a resistivity of 18.2 MΩ·cm was used throughout the experiment.

Synthesis of Ag Seeds 16−45 nm in Size. Cubic and quasi-spherical Ag seeds with sizes less than 30 nm were prepared using our recently reported protocol with DEG as the solvent/reductant.[14] In a typical synthesis, 5 mL of DEG was added into a three-necked flask (100 mL) and heated under magnetic stirring in an oil bath (150 °C) for 30 min. Other reagents dissolved in DEG were sequentially added into the flask using a pipet. Specifically, 0.06 mL of NaSH solution (3 mM) was first added. After 4 min, 0.5 mL of HCl (3 mM) was added, followed by 1.25 mL of PVP (20 mg/mL). After another 2 min, 0.4 mL of CF_3COOAg solution (282 mM) was added. During the entire process, the flask was capped with glass stoppers except for the addition of reagents. The sizes of the Ag seeds could be controlled by monitoring the positions of their main LSPR peaks

using a UV−vis spectrometer during their growth. The quasi-spherical single-crystal seeds of 16 nm in size were obtained by quenching the reaction with an ice−water bath when the LSPR peak was positioned at 398 nm. The cubic single-crystal seeds of 21 and 28 nm in size were obtained by quenching the reaction when the LSPR peaks were shifted to 405 and 413 nm, respectively. After centrifugation, the seeds were washed with acetone once and DI water three times before they were redispersed and stored in DI water at a concentration of 1.5×10^{13} particles/mL.

Cubic Ag seeds of 45 nm in size were prepared using the same protocol as 28 nm seeds described above, except for the use of EG as a solvent/reductant.[15] The product was obtained by quenching the reaction with an ice−water bath when the major LSPR peak had reached 440 nm. After centrifugation and washing with acetone and DI water three times, the seeds were then redispersed in DI water or EG at a concentration of 1.1×10^{12} particles/mL for further use. Quasi-spherical Ag seeds of 35 nm in size were prepared by etching the 45-nm Ag nanocubes. Specifically, 0.2 mL of the as-obtained Ag nanocubes (45 nm, dispersed in EG) was added into a 25 mL flask containing 5 mL of EG, and heated to 150 °C under magnetic stirring. Then, 50 mM HCl (in EG) was added, and the final concentration of HCl in the solution was 1 mM. The mixture was heated for an additional 5 min, and cooled down to room temperature. Finally, after centrifugation and washing with acetone and DI water three times, the product was redispersed in DI water at a concentration of 1.1×10^{12} particles/mL.

Multiply twinned Ag seeds were prepared using the standard procedure with DEG as a solvent and reductant,[14] except for the absence of NaSH and HCl. The seeds were obtained by quenching the reaction with an ice−water bath at $t = 5$ min after the injection of Ag precursor, followed by washing with acetone once and DI water three times before use.

Synthesis of Ag Octahedra. In a standard synthesis, 1.0 mL of aqueous Na_3CA (50 mM) was mixed with 1.5 mL of DI water in a 20-mL glass vial. After that, 20 μL of the as-prepared Ag seeds were injected with a pipet, followed by the addition of 0.1 mL of aqueous AA (50 mM). Then, a specific (as indicated in the figure caption) amount of aqueous CF_3COOAg (0.3 mM) was added into the mixture using a syringe pump at a rate of 2.0 mL/h under magnetic stirring. After the precursor had been added into the mixture, the reaction was allowed to continue for 5 min. The product was collected by centrifugation and washing with DI water three times.

Synthesis of Au Octahedral Nanocages. In a typical synthesis, 100 μL of the as-prepared Ag octahedra were dispersed in 5 mL of PVP (1 mg/mL), and heated to 90 °C under magnetic stirring. Then, a specific (as indicated in the figure caption) amount of $HAuCl_4$ aqueous solution (0.1 mM) was added using a syringe pump at a rate of 5 mL/h. We recorded the UV−vis spectra to track the progress of the reaction as the volume of $HAuCl_4$ solution was increased. Once cooled down to room temperature, the products were washed with 10 mL of saturated NaCl solution to remove AgCl. Then, they were collected by centrifugation and washing with DI water three times, and dispersed in DI water for further characterization.

Instrumentation. Transmission electron microscopy (TEM) images were taken using Hitachi H-7500 and HT7700 microscopes operated at 75 and 120 kV, respectively. High-resolution transmission electron microscopy (HRTEM) images were taken using an FEI Tecnai F30 High Resolution Electron Microscope operated at 300 kV. Scanning electron microscopy (SEM) images were captured using an FEI Nova NanoSEM 200 field-emission microscope operated at 15 kV. Extinction spectra of Ag nanocrystals and Au nanocages were recorded by a UV−vis spectrometer (Varian, Cary 50). The concentration of Ag was determined using a Perkin-Elmer inductively coupled plasma mass spectrometer (ICP-MS, NexION 300Q), and then converted into the concentration of Ag seeds once the particle size had been determined by TEM imaging.

Conflict of Interest: The authors declare no competing financial interest.

Acknowledgment. This work was supported in part by a grant from NSF (DMR-1215034) and startup funds from Georgia Institute of Technology. As a jointly supervised Ph.D. student from Southwest University, Y. Wang was also partially supported by a Fellowship from the China Scholarship Council (CSC). Part of the research was conducted at the Robert P. Apkarian Integrated Electron Microscopy Core of Emory University.

Supporting Information Available: TEM images of Ag polyhedrons at different tilting angles relative to electron beam; TEM images of Ag octahedra together with irregular Ag nanoparticles obtained from the cubic and quasi-spherical seeds, respectively; typical HRTEM images of the seeds and the resultant products; TEM images of multiply twinned Ag seeds and the corresponding product obtained *via* seed-mediated growth; models for calculation of the edge lengths of an octahedron grown from a cubic or a quasi-spherical Ag seed under an ideal situation; UV−vis spectra of the Ag seeds; TEM image of Ag nanocrystals obtained in the presence of citrate as a capping agent at a concentration lower than the standard synthesis; TEM image of products obtained with the use of Ag octahedra as seeds; TEM image of Au fragments obtained with the addition of too much $HAuCl_4$ solution into the suspension of Ag octahedra. This material is available free of charge *via* the Internet at http://pubs.acs.org.

REFERENCES AND NOTES

1. Christopher, P.; Linic, S. Engineering Selectivity in Heterogeneous Catalysis: Ag Nanowires as Selective Ethylene Epoxidation Catalysts. *J. Am. Chem. Soc.* **2008**, *130*, 11264–11265.
2. Christopher, P.; Linic, S. Shape- and Size-Specific Chemistry of Ag Nanostructures in Catalytic Ethylene Epoxidation. *ChemCatChem* **2010**, *2*, 78–83.
3. Jiang, Z.-J.; Liu, C.-Y.; Sun, L.-W. Catalytic Properties of Silver Nanoparticles Supported on Silica Spheres. *J. Phys. Chem. B* **2005**, *109*, 1730–1735.
4. Kumar, A.; Vemula, P. K.; Ajayan, P. M.; John, G. Silver-Nanoparticle-Embedded Antimicrobial Paints Based on Vegetable Oil. *Nat. Mater.* **2008**, *7*, 236–241.
5. Rai, M. K.; Deshmukh, S. D.; Ingle, A. P.; Gade, A. K. Silver Nanoparticles: The Powerful Nanoweapon against Multidrug-Resistant Bacteria. *J. Appl. Microbiol.* **2012**, *112*, 841–852.
6. Nie, S.; Emory, S. R. Probing Single Molecules and Single Nanoparticles by Surface-Enhanced Raman Scattering. *Science* **1997**, *275*, 1102–1106.
7. Anker, J. N.; Hall, W. P.; Lyandres, O.; Shah, N. C.; Zhao, J.; Van Duyne, R. P. Biosensing with Plasmonic Nanosensors. *Nat. Mater.* **2008**, *7*, 442–453.
8. Rycenga, M.; Cobley, C. M.; Zeng, J.; Li, W.; Moran, C. H.; Zhang, Q.; Qin, D.; Xia, Y. Controlling the Synthesis and Assembly of Silver Nanostructures for Plasmonic Applications. *Chem. Rev.* **2011**, *111*, 3669–3712.
9. McLellan, J. M.; Li, Z.-Y.; Siekkinen, A. R.; Xia, Y. The SERS Activity of a Supported Ag Nanocube Strongly Depends on Its Orientation Relative to Laser Polarization. *Nano Lett.* **2007**, *7*, 1013–1017.
10. Xia, X.; Zeng, J.; McDearmon, B.; Zheng, Y.; Li, Q.; Xia, Y. Silver Nanocrystals with Concave Surfaces and Their Optical and Surface-Enhanced Raman Scattering Properties. *Angew. Chem., Int. Ed.* **2011**, *50*, 12542–12546.
11. Wiley, B. J.; Chen, Y.; McLellan, J. M.; Xiong, Y.; Li, Z.-Y.; Ginger, D.; Xia, Y. Synthesis and Optical Properties of Silver Nanobars and Nanorice. *Nano Lett.* **2007**, *7*, 1032–1036.
12. Xia, Y.; Xiong, Y.; Lim, B.; Skrabalak, S. E. Shape-Controlled Synthesis of Metal Nanocrystals: Simple Chemistry Meets Complex Physics?. *Angew. Chem., Int. Ed.* **2009**, *48*, 60–103.
13. Wiley, B.; Sun, Y.; Mayers, B.; Xia, Y. Shape-Controlled Synthesis of Metal Nanostructures: The Case of Silver. *Chem.—Eur. J.* **2005**, *11*, 454–463.
14. Wang, Y.; Zheng, Y.; Huang, C. Z.; Xia, Y. Synthesis of Ag Nanocubes 18−32 nm in Edge Length: The Effects of Polyol on Reduction Kinetics, Size Control, and Reproducibility. *J. Am. Chem. Soc.* **2013**, *135*, 1941–1951.
15. Zhang, Q.; Li, W.; Wen, L.-P.; Chen, J.; Xia, Y. Facile Synthesis of Ag Nanocubes of 30 to 70 nm in Edge Length with

CF_3COOAg as a Precursor. *Chem.—Eur. J.* **2010**, *16*, 10234–10239.
16. Zhang, Q.; Li, W.; Moran, C.; Zeng, J.; Chen, J.; Wen, L.-P.; Xia, Y. Seed-Mediated Synthesis of Ag Nanocubes with Controllable Edge Lengths in the Range of 30−200 nm and Comparison of Their Optical Properties. *J. Am. Chem. Soc.* **2010**, *132*, 11372–11378.
17. Sun, Y.; Xia, Y. Large-Scale Synthesis of Uniform Silver Nanowires through a Soft, Self-Seeding, Polyol Process. *Adv. Mater.* **2002**, *14*, 833–837.
18. Wiley, B.; Sun, Y.; Xia, Y. Polyol Synthesis of Silver Nanostructures: Control of Product Morphology with Fe(II) or Fe(III) Species. *Langmuir* **2005**, *21*, 8077–8080.
19. Xia, Y.; Xia, X.; Wang, Y.; Xie, S. Shape-Controlled Synthesis of Metal Nanocrystals. *MRS Bull.* **2013**, *38*, 335–344.
20. Jin, R.; Cao, Y. C.; Hao, E.; Metraux, G. S.; Schatz, G. C.; Mirkin, C. A. Controlling Anisotropic Nanoparticle Growth through Plasmon Excitation. *Nature* **2003**, *425*, 487–490.
21. Millstone, J. E.; Hurst, S. J.; Metraux, G. S.; Cutler, J. I.; Mirkin, C. A. Colloidal Gold and Silver Triangular Nanoprisms. *Small* **2009**, *5*, 646–664.
22. Zhang, J.; Langille, M. R.; Mirkin, C. A. Synthesis of Silver Nanorods by Low Energy Excitation of Spherical Plasmonic Seeds. *Nano Lett.* **2011**, *11*, 2495–2498.
23. Tao, A.; Sinsermsuksakul, P.; Yang, P. Polyhedral Silver Nanocrystals with Distinct Scattering Signatures. *Angew. Chem., Int. Ed.* **2006**, *45*, 4597–4601.
24. Tao, A. R.; Ceperley, D. P.; Sinsermsuksakul, P.; Neureuther, A. R.; Yang, P. Self-Organized Silver Nanoparticles for Three-Dimensional Plasmonic Crystals. *Nano Lett.* **2008**, *8*, 4033–4038.
25. Mulvihill, M. J.; Ling, X. Y.; Henzie, J.; Yang, P. Anisotropic Etching of Silver Nanoparticles for Plasmonic Structures Capable of Single-Particle SERS. *J. Am. Chem. Soc.* **2010**, *132*, 268–274.
26. Henzie, J.; Grünwald, M.; Widmer-Cooper, A.; Geissler, P. L.; Yang, P. Self-Assembly of Uniform Polyhedral Silver Nanocrystals into Densest Packings and Exotic Superlattices. *Nat. Mater.* **2012**, *11*, 131–137.
27. Tsuji, M.; Maeda, Y.; Hikino, S.; Kumagae, H.; Matsunaga, M.; Tang, X.-L.; Matsuo, R.; Ogino, M.; Jiang, P. Shape Evolution of Octahedral and Triangular Platelike Silver Nanocrystals from Cubic and Right Bipyramidal Seeds in DMF. *Cryst. Growth Des.* **2009**, *9*, 4700–4705.
28. Zeng, J.; Zhu, C.; Tao, J.; Jin, M.; Zhang, H.; Li, Z.-Y.; Zhu, Y.; Xia, Y. Controlling the Nucleation and Growth of Silver on Palladium Nanocubes by Manipulating the Reaction Kinetics. *Angew. Chem., Int. Ed.* **2012**, *51*, 2354–2358.
29. Ghosh, S. K.; Kundu, S.; Mandal, M.; Nath, S.; Pal, T. Studies on the Evolution of Silver Nanoparticles in Micelle by UV-Photoactivation. *J. Nanopart. Res.* **2003**, *5*, 577–587.
30. Heinz, H.; Farmer, B. L.; Pandey, R. B.; Slocik, J. M.; Patnaik, S. S.; Pachter, R.; Naik, R. R. Nature of Molecular Interactions of Peptides with Gold, Palladium, and Pd-Au Bimetal Surfaces in Aqueous Solution. *J. Am. Chem. Soc.* **2009**, *131*, 9704–9714.
31. Coppage, R.; Slocik, J. M.; Briggs, B. D.; Frenkel, A. I.; Heinz, H.; Naik, R. R.; Knecht, M. R. Crystallographic Recognition Controls Peptide Binding for Bio-Based Nanomaterials. *J. Am. Chem. Soc.* **2011**, *133*, 12346–12349.
32. Ruan, L.; Ramezani-Dakhel, H.; Chiu, C.-Y.; Zhu, E.; Li, Y.; Heinz, H.; Huang, Y. Tailoring Molecular Specificity Toward a Crystal Facet: A Lesson From Biorecognition Toward Pt{111}. *Nano Lett.* **2013**, *13*, 840–846.
33. Zeng, J.; Zheng, Y.; Rycenga, M.; Tao, J.; Li, Z.-Y.; Zhang, Q.; Zhu, Y.; Xia, Y. Controlling the Shapes of Silver Nanocrystals with Different Capping Agents. *J. Am. Chem. Soc.* **2010**, *132*, 8552–8553.
34. Kilin, D. S.; Prezhdo, O. V.; Xia, Y. Shape-Controlled Synthesis of Silver Nanoparticles: Ab Initio Study of Preferential Surface Coordination with Citric Acid. *Chem. Phys. Lett.* **2008**, *458*, 113–116.
35. Tao, A. R.; Habas, S.; Yang, P. Shape Control of Colloidal Metal Nanocrystals. *Small* **2008**, *4*, 310–325.
36. Jin, M.; Zhang, H.; Xie, Z.; Xia, Y. Palladium Nanocrystals Enclosed by {100} and {111} Facets in Controlled Proportions and Their Catalytic Activities for Formic Acid Oxidation. *Energy Environ. Sci.* **2012**, *5*, 6352–6357.
37. Xia, X.; Zeng, J.; Oetjen, L. K.; Li, Q.; Xia, Y. Quantitative Analysis of the Role Played by Poly(vinylpyrrolidone) in Seed-Mediated Growth of Ag Nanocrystals. *J. Am. Chem. Soc.* **2012**, *134*, 1793–1801.
38. Yang, W.-H.; Schatz, G. C.; Van Duyne, R. P. Discrete Dipole Approximation for Calculating Extinction and Raman Intensities for Small Particles with Arbitrary Shapes. *J. Chem. Phys.* **1995**, *103*, 869–875.
39. Wiley, B. J.; Im, S. H.; Li, Z.-Y.; McLellan, J.; Siekkinen, A.; Xia, Y. Maneuvering the Surface Plasmon Resonance of Silver Nanostructures through Shape-Controlled Synthesis. *J. Phys. Chem. B* **2006**, *110*, 15666–15675.
40. Sun, Y.; Mayers, B.; Herricks, T.; Xia, Y. Polyol Synthesis of Uniform Silver Nanowires: A Plausible Growth Mechanism and the Supporting Evidence. *Nano Lett.* **2003**, *3*, 955–960.
41. Niu, Z.; Zhen, Y.-R.; Gong, M.; Peng, Q.; Nordlander, P.; Li, Y. Pd Nanocrystals with Single-, Double-, and Triple-Cavities: Facile Synthesis and Tunable Plasmonic Properties. *Chem. Sci.* **2011**, *2*, 2392–2395.
42. Hong, X.; Wang, D.; Cai, S.; Rong, H.; Li, Y. Single-Crystalline Octahedral Au−Ag Nanoframes. *J. Am. Chem. Soc.* **2012**, *134*, 18165–18168.
43. Mahmoud, M. A.; Saira, F.; El-Sayed, M. A. Experimental Evidence for the Nanocage Effect in Catalysis with Hollow Nanoparticles. *Nano Lett.* **2010**, *10*, 3764–3769.
44. Xia, Y.; Li, W.; Cobley, C. M.; Chen, J.; Xia, X.; Zhang, Q.; Yang, M.; Cho, E. C.; Brown, P. K. Gold Nanocages: From Synthesis to Theranostic Applications. *Acc. Chem. Res.* **2011**, *44*, 914–924.
45. Yavuz, M. S.; Cheng, Y.; Chen, J.; Cobley, C. M.; Zhang, Q.; Rycenga, M.; Xie, J.; Kim, C.; Song, K. H.; Schwartz, A. G.; Wang, L. V.; Xia, Y. Gold Nanocages Covered by Smart Polymers for Controlled Release with Near-Infrared Light. *Nat. Mater.* **2009**, *8*, 935–939.
46. Wang, Y.; Liu, Y.; Luehmann, H.; Xia, X.; Wan, D.; Cutler, C.; Xia, Y. Radioluminescent Gold Nanocages with Controlled Radioactivity for Real-Time *in Vivo* Imaging. *Nano Lett.* **2013**, *13*, 581–585.
47. Zeng, J.; Zhang, Q.; Chen, J.; Xia, Y. A Comparison Study of the Catalytic Properties of Au-Based Nanocages, Nanoboxes, and Nanoparticles. *Nano Lett.* **2010**, *10*, 30–35.
48. Rycenga, M.; Hou, K. K.; Cobley, C. M.; Schwartz, A. G.; Camargo, P. H. C.; Xia, Y. Probing the Surface-Enhanced Raman Scattering Properties of Au−Ag Nanocages at Two Different Excitation Wavelengths. *Phys. Chem. Chem. Phys.* **2009**, *11*, 5903–5908.
49. Chen, J.; McLellan, J. M.; Siekkinen, A.; Xiong, Y.; Li, Z.-Y.; Xia, Y. Facile Synthesis of Gold-Silver Nanocages with Controllable Pores on the Surface. *J. Am. Chem. Soc.* **2006**, *128*, 14776–14777.
50. Sun, Y.; Xia, Y. Mechanistic Study on the Replacement Reaction between Silver Nanostructures and Chloroauric Acid in Aqueous Medium. *J. Am. Chem. Soc.* **2004**, *126*, 3892–3901.
51. Chen, J.; Wiley, B.; McLellan, J.; Xiong, Y.; Li, Z.-Y.; Xia, Y. Optical Properties of Pd-Ag and Pt-Ag Nanoboxes Synthesized *via* Galvanic Replacement Reactions. *Nano Lett.* **2005**, *5*, 2058–2062.
52. Dick, K.; Dhanasekaran, T.; Zhang, Z.; Meisel, D. Size-Dependent Melting of Silica-Encapsulated Gold Nanoparticles. *J. Am. Chem. Soc.* **2002**, *124*, 2312–2317.
53. Shi, H.; Zhang, L.; Cai, W. Composition Modulation of Optical Absorption in Ag_xAu_{1-x} Alloy Nanocrystals in sSitu Formed within Pores of Mesoporous Silica. *J. Appl. Phys.* **2000**, *87*, 1572–1574.